

Article

Effect of Process Parameters on the Microstructure and Wear Resistance of Fe₃Al/Cr₃C₂ Composites

Yaohui Wang ^{1,2}, Yingkai Feng ^{3,*}, Xiaohu Sun ², Shaoquan Liu ^{3,*} and Guoqiang Chen ⁴¹ School of Mechanical, Electrical and Control Engineering, Beijing Jiaotong University, Beijing 100044, China² Huaneng Coal Technology Research Co., Ltd., Beijing 100070, China; xh_sun@chnng.com.cn³ Chinese Institute of Coal Science, Beijing 100013, China⁴ Huaneng Coal Industry Co., Ltd., Beijing 100070, China

* Correspondence: fengyingkai1029@126.com (Y.F.); 13020003390@163.com (S.L.)

Abstract: In this paper, a brake cylinder coating comprising a composite material of an Fe₃Al and Cr₃C₂ mixed powder was prepared by adding laser cladding onto carbon structural steel. We studied the influence of process parameters on the microstructure and tribological properties of the cladding materials using scanning electron microscopy (SEM), energy-dispersive spectroscopy (EDS), and 3D white light interferometer and wear tests. The influence of different processes on the morphology of the carbide strengthening phase was found to be relatively small with a Cr₃C₂ content of 15 wt.%. The carbides mainly exhibited a network structure in each group of cladding layers. The area of the network strengthening phase varied under different processes. Of the cladding layers formed with different processes, the scanning speed of the 0.003 m/s cladding layer had the lowest wear rate. When the laser power was too low or the powder feed rate was too high, unmelted Cr₃C₂ particles could be found in the cladding layer. During the wear process, the particles peeled off, causing severe abrasive wear. When the powder feeding rate was too low, more materials in the base material entered the cladding layer. This made the composition of the cladding layer similar to that of the grinding material, resulting in severe adhesive wear.



Citation: Wang, Y.; Feng, Y.; Sun, X.; Liu, S.; Chen, G. Effect of Process Parameters on the Microstructure and Wear Resistance of Fe₃Al/Cr₃C₂ Composites. *Coatings* **2024**, *14*, 384. <https://doi.org/10.3390/coatings14040384>

Academic Editors: Jordan Todorov Maximov and Galya Velikova Duncheva

Received: 24 February 2024
Revised: 21 March 2024
Accepted: 22 March 2024
Published: 25 March 2024



Copyright: © 2024 by the authors. Licensee MDPI, Basel, Switzerland. This article is an open access article distributed under the terms and conditions of the Creative Commons Attribution (CC BY) license (<https://creativecommons.org/licenses/by/4.0/>).

Keywords: carbide behavior; Fe₃Al/Cr₃C₂ composites; laser cladding; process parameter

1. Introduction

Coal is an important energy source in China. With the continuous development of the national economy, the demand for coal is increasing day by day. Increasingly heavy mining tasks have brought about severe challenges for mechanical equipment. Therefore, the development and application of high-strength, wear-resistant materials is urgent. Fe₃Al alloy and its composite materials have good resistance against wear, high temperatures, and oxidation [1–6]. Due to the high content of Fe and Al in the Earth's crust and the low cost of these two elements, the large-scale application of Fe₃Al also has particularly high economic value.

However, currently, the brittleness of Fe₃Al at room temperature limits its performance in practical applications [7–9]. In recent years, researchers have been committed to toughening Fe₃Al through various methods to overcome its brittleness problem. The main improvement method is to add elements for alloying. In the alloying of Fe₃Al, more research has been conducted on using Cr and B elements to solve the problem of high brittleness. The mechanism of action of the two elements is not the same. Cr is a solid solution softening element that can improve the plasticity of alloys and increase toughness [10]. It has been found that a lower content of B and Zr elements can significantly improve the toughness of Ni₃Al and Fe₃Al [11,12]. In order to further enhance the wear resistance and improve the plasticity of Fe₃Al, Cr₃C₂ was used as the strengthening phase to prepare Fe₃Al composite materials.

Cr_3C_2 is often used as a strengthening phase in composite materials due to its high thermal hardness, good corrosion resistance, high oxidation resistance, and compatibility with the thermal expansion coefficient of most alloys [13–15]. Therefore, the addition of Cr_3C_2 to the matrix as a hard-strengthening phase will greatly improve the wear resistance of the material. Composite materials, due to the combination of the excellent properties of several materials, can achieve higher performance at a lower cost [16]. Yuan et al. [17] investigated the effect of Cr_3C_2 content (3 wt.%, 6 wt.%, and 9 wt.%) on the microstructure and mechanical properties of composite materials. Their results indicated that adding an appropriate amount of Cr_3C_2 to a WC-Co hard alloy can effectively suppress the abnormal growth of WC grains, improve grain uniformity, and reduce microstructural defects, thereby improving its comprehensive mechanical properties. This indicates that Cr_3C_2 can serve as an excellent strengthening phase for composite materials and can improve the performance of alloys. Liu et al. [18] prepared a $\text{Ni}_3\text{Al}/\text{Cr}_3\text{C}_2$ -composite wear-resistant coating on a 42CrMo base material, and proposed a wear model of the composite material based on the results of experiments on friction and wear. This model proposes a softer Ni_3Al phase as the base, with harder carbide particles embedded in it. During the wear process, the hard particles isolate the absolute wear pair, thereby reducing the overall wear of the material.

Laser cladding is a new surface modification technology. It uses a high-energy-density laser beam to fuse cladding material with a thin layer on the surface of a base material. The cladding layer has low dilution and is metallurgically bonded with the base material. It can significantly improve the wear resistance, corrosion resistance, heat resistance, anti-oxidation, or electrical properties of the surface of a substrate material, thereby achieving the purpose of surface modification or repair. It can save a great deal of material costs while meeting the specific performance requirements of the material surface [19–21].

The process parameters of laser cladding include powder feed rate, laser power, scanning rate, etc. The different cladding processes can change the dilution rate of a cladding layer, which may affect the morphology of the carbide strengthening phase in the microstructure [22]. Changes in the cladding process will inevitably have a significant impact on the wear resistance of a cladding layer. Therefore, analyzing the influence of the cladding process on a cladding layer and exploring the wear mechanism of laser cladding $\text{Fe}_3\text{Al}/\text{Cr}_3\text{C}_2$ composite materials are of great significance.

The research on Fe_3Al alloy and Fe_3Al matrix composite materials has mainly focused on $\text{Fe-Al}/\text{Al}_2\text{O}_3$, $\text{Fe-Al}/\text{WC}$, and other such composite materials. In the research on $\text{Fe-Al}/\text{Cr}_3\text{C}_2$ composite materials, only thermal spraying coating technology has been considered in detail. Systematic investigations on the wear resistance of an $\text{Fe}_3\text{Al}/\text{Cr}_3\text{C}_2$ cladding layer, as well as on the influence of process parameters on the properties of the $\text{Fe}_3\text{Al}/\text{Cr}_3\text{C}_2$ composite and on the friction and wear mechanism of the $\text{Fe}_3\text{Al}/\text{Cr}_3\text{C}_2$ composite laser, are still lacking. Compared with previous studies, the main novelty of this work is that we studied the influence of process parameters on the microstructure of the cladding layer and the effect mechanism of process parameters on the wear resistance of $\text{Fe}_3\text{Al}/\text{Cr}_3\text{C}_2$ composites.

2. Method

2.1. Preparation of Cladding Layer

Carbon structural steel was used as the base material. The chemical composition of Fe_3Al powder is shown in Table 1. The cladding powder was a mixture of an Fe_3Al and Cr_3C_2 powder with a 75–125 μm particle size. The Cr_3C_2 powder was prepared by crushing a large block of commercial pure Cr_3C_2 block. The chemical composition of the Fe_3Al powder is shown in Table 2.

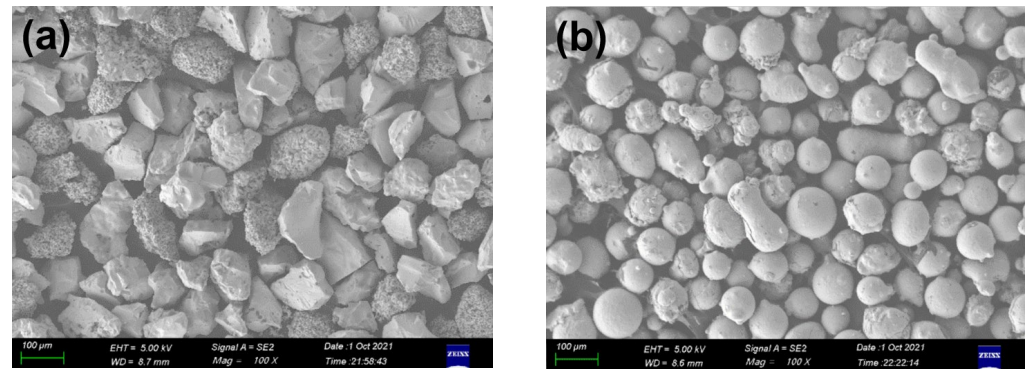
Table 1. Chemical composition of the base material (wt.%).

C	Si	Mn	Cr	Ni	Fe
0.45	0.2	0.66	0.24	0.28	98.17

Table 2. Chemical composition of the Fe₃Al powder (wt.%).

Al	B	Cr	Fe	Mn	Ni	Zr
15.23	0.11	5.78	76.82	0.052	0.54	0.26

Aluminum blocks and iron powder (CISRI, Beijing, China) were melted in a vacuum furnace at 1900~2000 °C for 1 h and then atomized into powder. The morphology of the two powders is shown in Figure 1.

**Figure 1.** SEM morphology of the Fe₃Al and Cr₃C₂ powder. (a) Cr₃C₂ powder. (b) Fe₃Al powder.

We chose 15 wt.% for the Cr₃C₂ content of the cladding layer because previous research [22] has proven that the coating has less of a tendency to crack at this content. Through pre-experiments, we determined the optimal process range for the forming. The scanning speed selection was 0.002 m/s–0.004 m/s. The laser power selection was 1.8 kW–2.6 kW. The powder feeding rate selection was 0.429 kg/h–0.966 kg/h. We obtained the optimal forming process with a laser power of 2.2 kW, a scanning rate of 0.002 m/s, and a powder feeding rate of 0.644 kg/h. The parameters of each process group that were finally determined for analysis are shown in Table 3.

Table 3. Process parameters for each group.

Group	Laser Power (kW)	Scanning Rate (m/s)	Powder Feed Rate (kg/h)	Cr ₃ C ₂ Content
1	2.2	0.002	0.644	15 wt.%
2	2.2	0.003	0.644	15 wt.%
3	2.2	0.004	0.644	15 wt.%
4	1.8	0.002	0.644	15 wt.%
5	2.6	0.002	0.644	15 wt.%
6	2.2	0.002	0.966	15 wt.%
7	2.2	0.002	0.429	15 wt.%

We use laser cladding as the molding process and use YLS-6000 fiber lasers (IPG Photonic, Oxford, MA, USA). The installation platform of the laser was the KUKA robotic arm, which formed a forming system together with the powder feeder. The laser wavelength was 1.07 µm. We selected a Gaussian distribution focusing lens for the laser head to generate a rectangular laser spot with a size of 2 mm × 5 mm. The powder feeding type was coaxial powder feeding, the shielding gas and powder carrying gas were high-purity argon (99.99%), and the flow of shielding gas was 15 L/min. In order to ensure the efficiency and quality of the forming, we used 240# sandpaper before the cladding to remove impurities and dirt from the surface of the base material. We then cleaned it with acetone to reduce the brightness of the base material, as well as to remove the oil and oxides on the surface.

2.2. Microstructure Characterization

We obtained the cross-section of the cladding layer via wire cutting along the direction that was perpendicular to the cladding layer. The sample sizes were 10 mm × 10 mm, which was the full thickness of the section. In turn, we polished the section with 80#, 240#, 600#, and 1000# sandpaper, and we then polished the sample with a 2.5 μm diamond polishing agent. The hardness of the cladding layer was measured with an FM300 microhardness tester (F-T, Tokyo, Japan). In order to observe the microstructure of the cladding layer, a Zeiss high-resolution field emission scanning electron microscope (SEM, ZEISS, Jena, Germany) was used to observe the cross-section of the cladding layer.

2.3. Wear Test

The wear test was conducted using a UMT-3 controllable environmental friction and wear tester (UMT, BRUKER, Madison, MA, USA). The friction type was a pin disk surface-contact cyclic friction. In the test, the bottom of the pin was the prepared Fe₃Al/Cr₃C₂ cladding layer. The gray cast iron grinding discs were made by cutting the inner wall of the engine with a size of Ø 24 mm × 7.88 mm. The wear test conditions were as follows: dry friction, a load of 20 N, a rotation radius of 7 mm, a rotation speed of 200 r/min, a static pressure load of 20 N, and a testing time of 120 min. In order to obtain more accurate mass data before and after wear, the pins and discs were ultrasonically cleaned with acetone for 10 min. The mass was measured using a high-precision analytical balance, and the pin mass before test M_1 and mass after test M_2 were recorded. The wear loss was calculated using $M = M_1 - M_2$.

3. Result

The macroscopic morphology of each group of cladding layers after forming is shown in Figure 2. The part of the cladding layer that was 1 mm away from the base material was selected for etching. The morphology is shown in Figure 3.



Figure 2. Macromorphology of the cladding layers after forming with different processes. (a) The optimal forming process; (b) a scanning speed of 0.003 m/s; (c) a scanning speed of 0.004 m/s; (d) a laser power of 1.8 kW; (e) a laser power of 2.6 kW; (f) a powder feed rate of 0.429 kg/h; and (g) a powder feed rate of 0.966 kg/h.

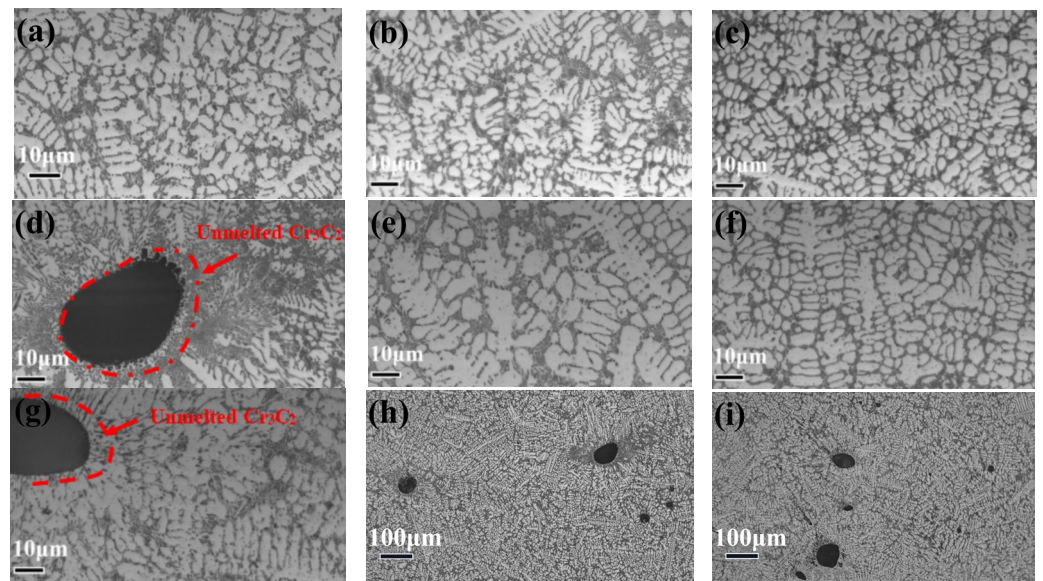


Figure 3. SEM morphology of the cladding layers prepared with different processes: (a) the optimal forming process; (b) a scanning speed of 0.003 m/s; (c) a scanning speed of 0.004 m/s; (d,h) a laser power of 1.8 kW; (e) a laser power of 2.6 kW; (f) a powder feed rate of 0.429 kg/h; and (g,i) a powder feed rate of 0.966 kg/h.

From Figure 2a–c, it can be seen that cladding layers with different scanning speeds had significant differences in melting height, and the forming of these cladding layers was relatively good and did not create any cracks.

From Figure 3a–c, it can be seen that, from the morphology of the carbide after etching, the internal microstructure of the three groups of cladding layers with different powder feeding rates was almost the same. The main two phases were the lighter-colored matrix phase and the darker-colored carbide phase. The carbide phase was distributed in the matrix phase as a network structure.

The group with the scanning speed of 0.002 m/s had a larger area of the network structure node, while the groups with a scanning speed of 0.003 m/s and 0.004 m/s had a more uniform distribution of the carbide phase and smaller nodes. From the area of the carbide phase, which is counted in Table 4, it can be seen that the carbide phase area reached its maximum value with a scanning speed of 0.002 m/s. As the scanning rate increased, the area of carbides gradually decreased.

Table 4. Proportion of the carbide area in the cladding layer with different processes.

Group	The Proportion of the Carbide Area
1	36.46%
2	31.98%
3	21.54%
4	26.26%
5	20.40%
6	22.13%
7	28.62%

From Figure 2a,d,e, it can be seen that the cladding layers with different laser power were well formed. However, when the laser power was 2.6 kW, the cladding layer cracked, and the cladding width was slightly wider. There were no cracks generated when the power was 1.8 kW and 2.2 kW.

From Figure 3a,d,e,h, it can be found that, after etching, the internal microstructure of the three, which contained the matrix phase and carbide phase, was almost the same.

The carbide phase nodes of the cladding layer with the laser power of 1.8 kW were the largest, with a relatively uneven distribution, and there were large unmelted Cr_3C_2 particles remaining. Unmelted Cr_3C_2 particles were not found in the 2.2 kW and 2.6 kW cladding layers. With the increase in laser power, the distribution of the carbide phase in the cladding layers with the laser powers of 2.2 kW and 2.6 kW gradually became uniform, and the carbide phase transformation was small in the large areas at node positions. The carbide phase distribution of the cladding layer with a laser power of 2.6 kW was sparse, and the number of dendrites inside the cladding layer increased.

From Figure 2a,f,g, it can be seen that the cladding layers with different powder feed rates did not produce significant differences in their macroscopic morphology, except for the melting height. The cladding layers were all well-formed, and there were no cracks generated.

From Figure 3a,f,g,i it can be seen that, after etching, the internal microstructure was almost the same with different powder feed rates. The groups with powder feed rates of 0.644 kg/h and 0.966 kg/h had a larger area of network nodes. When the powder feed rate was 0.966 kg/h, large unmelted Cr_3C_2 particles could be observed in the cladding layer. From the calculated areas of carbides shown in Table 3, it can be seen that the group with the maximum carbide phase area was the one with the powder feed rate of 0.644 kg/h. When the powder feed rate is smaller than 0.644 kg/h, the dilution rate of the cladding layer will be high, thus resulting in a decrease in the content of the carbide phase. When it is larger than 0.644 kg/h, the Cr_3C_2 particles in the cladding powder cannot be fully melted, thereby resulting in a decrease in the area of the network carbide phase.

Wear test samples were prepared from the previously determined seven groups of cladding layers. Then, the wear test was conducted and the following friction coefficient curve was obtained.

From Figure 4, it can be seen that, with the same Cr_3C_2 content, different processes had a significant impact on the friction coefficient. The groups with the larger friction coefficients were those with a laser power of 1.8 kW and a powder feed rate of 0.429 kg/h. The group with the lowest coefficient was the group with a scanning speed of 0.003 m/s. From the point of view of the friction coefficient fluctuation, except for the powder feed rate of 0.429 kg/h and 0.966 kg/h, the friction coefficient curve of the other groups was relatively stable. During the actual wear tests of the two groups with fluctuating friction coefficients, periodic loud noises could be heard.

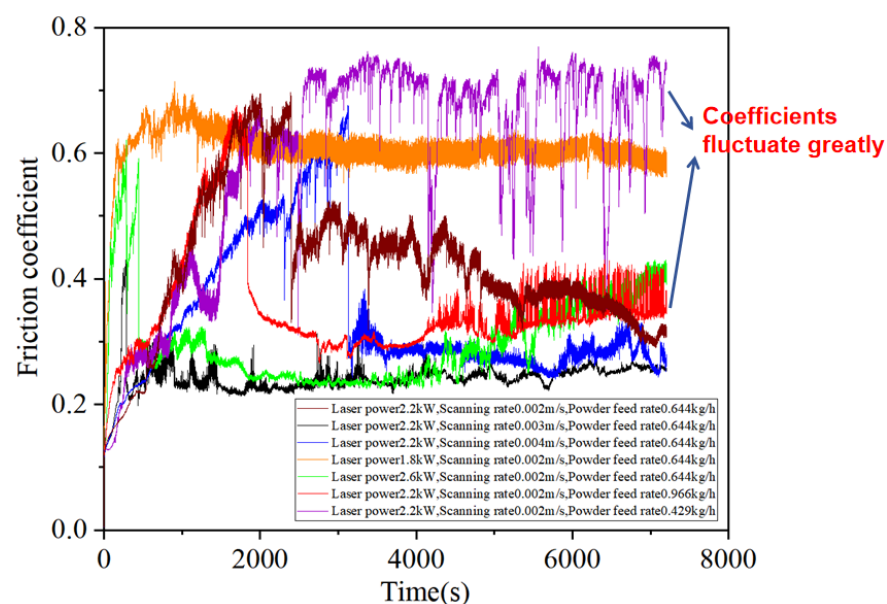


Figure 4. Friction coefficient curves of the cladding layers with different processes.

Although the correlation between the hardness, friction, and wear properties was not linear, it was positive [23–25]. Therefore, measuring the hardness of the cladding layer can reflect the wear resistance of the material to a certain extent. We carried out macroscopic hardness measurements for each group of cladding layers. The hardness value results are shown in Table 5, and the error range is $\pm 2\%$. It can be seen in Table 5 that the hardness of cladding layers with a powder delivery rate of 0.429 kg/h and a laser power of 2.6 kW was lower, and the hardness of other groups of cladding layers was not much different.

Table 5. Hardness of the cladding layers with different processes.

Group	Hardness (HRC)	Hardness (HV)
1	38.4	361.4
2	39.8	375.0
3	34.4	325.8
4	38.8	365.2
5	26.1	264.1
6	41.6	393.4
7	30.7	346.5

It can be seen from Table 6 that, except for the group with a powder feed rate of 0.429 kg/h, the wear rate exceeded $1 \times 10^{-5} \text{ mm}^3/\text{N}\cdot\text{m}$, and the other groups were lower than this value. There was still a large difference in the wear rate between different process parameter groups. Among them, Groups 1, 2, 4, and 6 had less wear, while Groups 3 and 5 had higher wear.

Table 6. Wear rate of cladding layers with different processes.

Group	Mass Lose (g)	Wear Rate ($1 \times 10^{-14} \text{ m}^3/\text{N}\cdot\text{m}$)
1	0.00239	0.396
2	0.00019	0.139
3	0.00037	0.253
4	0.00085	0.871
5	0.00040	0.293
6	0.00058	0.394
7	0.00226	1.653

In order to reflect the excellent friction and wear properties of the composite materials, the currently common wear-resistant material vermicular cast iron was used as a control group. Wear tests were conducted under the same experimental conditions, and the wear rate was compared with that of the optimal process group. The results are shown in Table 7. The wear rate of the vermicular cast iron reached $3.102 \times 10^{-5} \text{ mm}^3/\text{N}\cdot\text{m}$, which was 22.31 times higher than the optimal wear rate group. From the perspective of wear on the grinding disc, the optimal wear rate group had a much lower wear than the vermicular cast iron group, thus indicating that the composite materials can not only reduce their own wear rate, but also reduce the wear on the grinding pair. The wear resistance of Cr_3C_2 -reinforced Fe_3Al laser cladding material was found to be far superior to the commonly used wear-resistant material vermicular cast iron, which reflects its excellent performance and great development potential in wear-resistant materials.

Table 7. Wear rate of different wear-resistant materials.

	Vermicular Graphite	The Optimal Process Group for Wear Rate
Pin wear rate ($1 \times 10^{-14} \text{ m}^3/\text{N}\cdot\text{m}$)	3.102	0.139
Wear loss of disc (g)	0.00227	0.00083

A 3D white light interferometer was used to carry out the observation of the worn pins and discs, and the results are shown in Figure 5. From Figure 5, it can be observed that there were obvious furrows on the surface of the cladding layer with six different processes after wear, thus indicating significant abrasive wear. The furrow was the deepest in the group with a laser power of 1.8 kW. In addition to the obvious abrasive wear observed in the process with a powder feed rate of 0.429 kg/h, there were irregular depressions with obvious material loss on the surface of the grinding pin, thereby indicating that this cladding layer also suffered from serious adhesive wear.

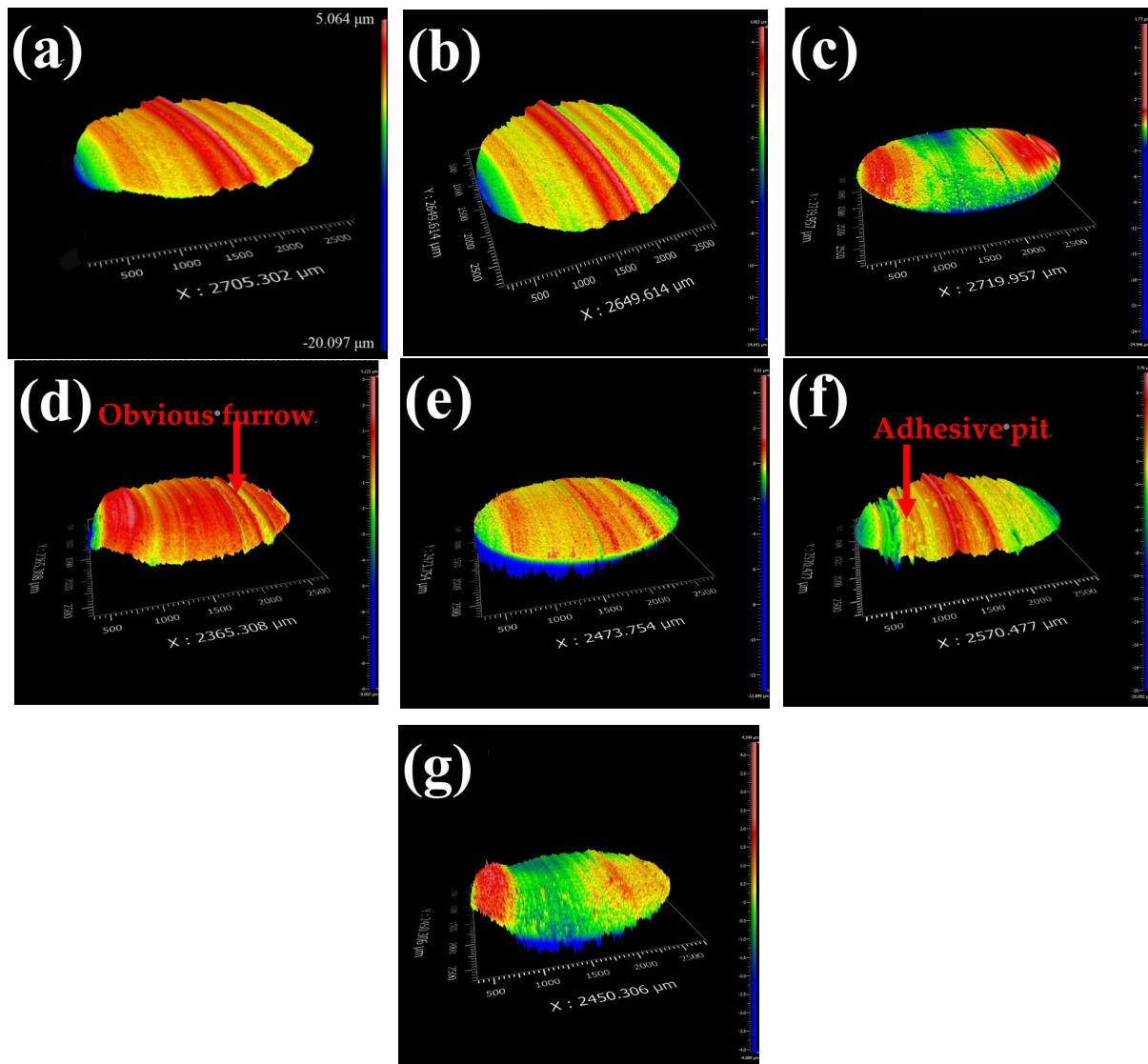


Figure 5. Three-dimensional profiles after wear of the grinding pins prepared with different processes: (a) the optimal forming process, (b) a scanning speed of 0.003 m/s, (c) a scanning speed of 0.004 m/s, (d) a laser power of 1.8 kW, (e) a laser power of 2.6 kW, (f) a powder feed rate 0.429 kg/h, and (g) a powder feed rate 0.966 kg/h.

Through SEM observations of the worn surfaces, as shown in Figure 6, it was found that the group with a laser power of 1.8 kw showed obvious furrows on the surface after wear. Meanwhile, the group with a powder feed rate of 0.429 kg/h showed adhesive pits on the surface after wear. These results were consistent with the white light interference results.

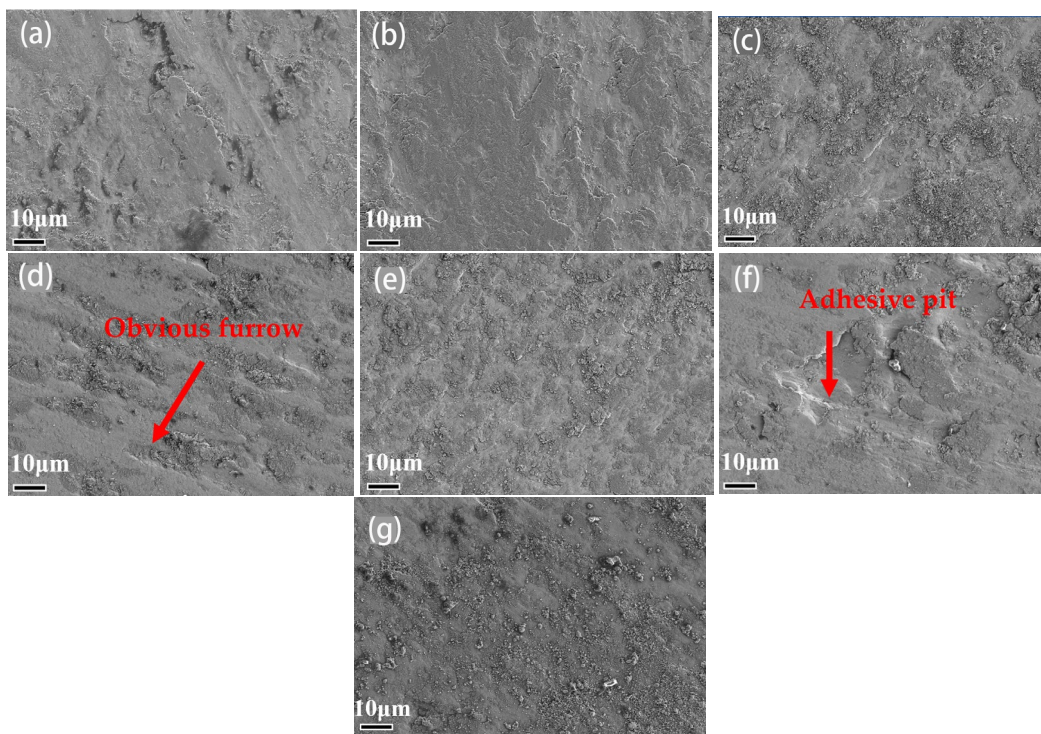


Figure 6. SEM morphology of grinding pin surfaces prepared with different processes: (a) the optimal forming process, (b) a scanning speed of 0.003 m/s, (c) a scanning speed of 0.004 m/s, (d) a laser power of 1.8 kW, (e) a laser power of 2.6 kW, (f) a powder feed rate 0.429 kg/h, and (g) a powder feed rate 0.966 kg/h.

4. Discussion

The hardness of the cladding layers with the same Cr_3C_2 content and different processes was not significantly different, except for those with a powder feed rate of 0.429 kg/h. When combining the wear rate results and the hardness of the cladding layer with different processes, a complete match between the two was not found. The 1.8 kW group was harder than the group with a scanning speed of 0.004 m/s, but their wear rate was higher.

Figure 3 shows that there was not much difference in the morphology and distribution of the strengthening phases in the cladding layers with different processes. Wear rates of all groups were relatively low, except for the two groups with a laser power of 1.8 kW and a powder feed rate of 0.429 kg/h. Based on the analysis of the microstructure morphology of the two groups with higher wear rates, it was found that the cladding layer with a laser power of 1.8 kW contained a large amount of unmelted Cr_3C_2 particles due to the low laser power during preparation. During the wear test, these large unmelted Cr_3C_2 particles, once worn down, would become large and hard abrasive particles, thereby greatly aggravating the abrasive wear between the grinding pin and disc [26,27]. The friction coefficient curve presented in Figure 4 can also support the analyzed wear mechanism. The friction coefficient of this group was always at a high level, and the surface underwent severe abrasive wear. The microstructure morphology of the cladding layer with a powder feed rate of 0.429 kg/h was not significantly different from the other groups. However, the hardness of this group was the lowest. Compared to the other groups, it experienced not only abrasive wear but also particularly severe adhesive wear. The friction coefficient curve showed that the coefficient of this group was relatively unstable as it sometimes suddenly decreased, thereby indicating a sudden change in the wear process, that is, the moment when the adhesive wear stuck the material down. Adhesive wear causes a large amount of material transfer in the cladding layer. Compared with the other groups, the group with a powder feeding rate of 0.429 kg/h had a smaller melting height and lower dilution rate.

Our analysis suggested that there was a significant relationship between a higher dilution rate and the occurrence of adhesive wear.

The range values can be obtained by calculating the mean values of each factor at various levels using the dilution rates of each cladding layer obtained via orthogonal experiment analysis, as shown in Table 8.

Table 8. Visual analysis table of the cladding layer dilution rate.

Influence Factor	Powder Feed Rate	Scanning Rate	Laser Power	Blank Column
Mean value1	0.225	0.166	0.115	0.142
Mean value2	0.173	0.115	0.123	0.142
Mean value3	0.119	0.117	0.129	0.061
Mean value4	0.093	0.138	0.149	0.175
Mean value5	0.087	0.162	0.181	0.193
range	0.138	0.051	0.066	0.132

From a visual analysis, it can be seen that the most important factor affecting the dilution rate of the cladding layer was the powder feed rate, and the range values of the other two factors were relatively small, thus indicating a lower degree of influence on the dilution rate. An effect curve was used to more intuitively analyze the influence of the powder feed rate on the dilution rate of a cladding layer.

From Figure 7, it can be seen that the dilution rate of the cladding layer gradually decreased with increasing powder feed. This was because, as the powder feeding rate increases, more laser energy is used to melt the powder, which reduces the energy that the base material can obtain and reduces the melting of the base material, thereby gradually reducing the dilution rate of the cladding layer. The lower powder feed rate resulted in a higher dilution rate in the group with a powder feed rate of 0.429 kg/h. Due to the similarity in material between the grinding disc and the base material steel, the excessive mass transfer from the base material steel to the cladding layer during the melting process increased the similarity between the material of the cladding layer and the material of the grinding disc. The Fe content of the pin could reflect the similarity between the pin and the grinding disc material. The higher the Fe content, the higher the similarity between the two materials. Table 9 shows the Fe content in the pins prepared by different process cladding layers. It can be seen from the table that the Fe content was the highest in the pins with a powder feed rate of 0.429 kg/h, which can be considered to be the most similar to the composition of gray cast iron grinding discs. Similar materials were prone to adhesive wear during wear, and this only resulted in severe adhesive wear in the group with a powder feed rate of 0.429 kg/h.

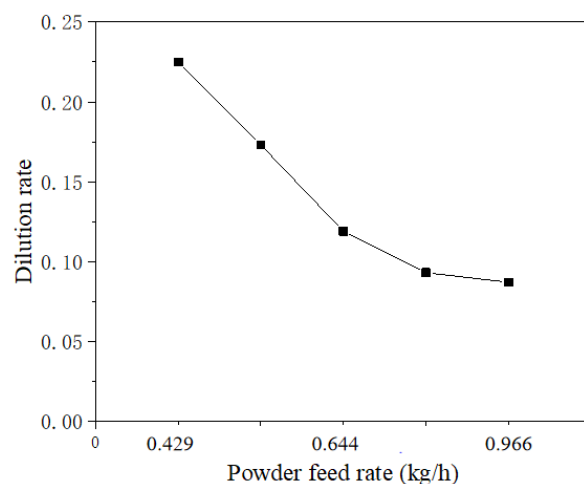


Figure 7. Effect curve of the cladding layer dilution rate.

Table 9. Fe content in pins with different processes.

Laser Power (kW)	Scanning Rate (m/s)	Powder Feed Rate (kg/h)	Fe Content (wt.%)
2.2	0.003	0.644	65.88
2.2	0.004	0.644	65.09
1.8	0.002	0.644	66.65
2.6	0.002	0.644	67.83
2.2	0.002	0.966	65.61
2.2	0.002	0.429	70.42

As shown in Table 6, even when severe abrasive wear occurred, the wear rate was lower than that of the adhesive wear. This was because the cutting effect of abrasive wear on the friction surface only caused the material to squeeze and move when facing materials with good plasticity; however, its contribution to the actual wear rate was not significant. The wear mechanism between the adhesive wear and abrasive wear was different. With respect to adhesive wear, the material directly adhered to the grinding pair and pulled away from the plane, thus causing material loss. This will also result in plastic materials losing weight in a relatively efficient way. When observing the wear rate of compacted graphite cast iron, which was previously used as a control group, it was found that its adhesive wear was more severe. The reason for this was that its material had good plasticity and was closer to the material of the grinding disc.

5. Conclusions

In this paper, the effects of the process parameters on the microstructure and wear resistance of a cladding layer were studied. The friction mechanism was further judged using white light interference and SEM observation. The friction and wear mechanisms were obtained by combining the test results with the microstructure.

1. The influence of different processes on the morphology of the carbide strengthening phase was relatively small with a Cr_3C_2 content of 15 wt.%. The carbides mainly exhibited a network structure in each group of cladding layers. The area of the network strengthening phase varied under different processes.
2. Judging by the visible furrows on the pin surface, abrasive wear appeared in all of the groups. Serious abrasive wear occurred in the pin with a laser power of 1.8 kW. Adhesive wear only occurred in the pin with a powder feed rate of 0.429 kg/h. The occurrence of adhesive wear or more serious abrasive wear will lead to greater wear. The cladding layer with a scanning speed of 0.003 m/s, which had the best wear resistance in all of the groups, had significant advantages in wear resistance compared to vermicular cast iron materials.
3. The influence mechanism of laser cladding process parameters on the wear resistance of the cladding layer was studied. When combining the wear rate results and the hardness of the cladding layer with different processes, a complete match between the two was not found. When the laser power was low, there were large unmelted Cr_3C_2 particles in the cladding layer. These particles will become large hard abrasive particles during the wear process, thereby resulting in severe abrasive wear and a higher wear rate. When the powder feed rate is low, it will cause the cladding layer to contain too much base material content and have a lower hardness. This makes the cladding layer prone to adhesive wear, thus greatly increasing the wear rate.

Author Contributions: Conceptualization, Y.W.; methodology, Y.F.; software, Y.F.; formal analysis, Y.F., S.L. and G.C.; writing—original draft, Y.F.; writing—review and editing, Y.W. and X.S. All authors have read and agreed to the published version of the manuscript.

Funding: This work was supported by the China Huaneng Group Technology Project (project no. HNKJ21-H56-06); the National Mine Safety Supervision Bureau Mine Safety Production Research and

Research Project (project no. 1-135-2023); and the Science and Technology Project of Coal Science Research Institute Co., Ltd. (project no. ZNKS20220401). The funder involved in the study design, collection.

Institutional Review Board Statement: Not applicable.

Informed Consent Statement: Not applicable.

Data Availability Statement: The raw data supporting the conclusions of this article will be made available by the authors on request.

Conflicts of Interest: Yaohui Wang and Xiaohu Sun were employed by the company Huaneng Coal Technology Research Co., Ltd. Guoqiang Chen was employed by the company Huaneng Coal Industry Co., Ltd. The remaining authors declare that the research was conducted in the absence of any commercial or financial relationships that could be construed as a potential conflict of interest.

References

- Luo, X.; Zhang, K.; Zhou, Y.; Wu, H.; Xie, H. In situ construction of Fe₃Al@Al₂O₃ core-shell particles with excellent electromagnetic absorption. *J. Colloid Interface Sci.* **2022**, *611*, 306–316. [CrossRef] [PubMed]
- Luo, X.; Xie, H.; Yu, F.; Cao, J.; Zhang, Y.; Lei, Z.; Zhang, K. Optimizing the order degree of plate-like Fe₃Al for high-performance electromagnetic wave absorption. *J. Mater. Sci. Mater. Electron.* **2023**, *34*, 2015. [CrossRef]
- Stoloff, N.S. Iron aluminides: Present status and future prospects. *Mater. Sci. Eng. A* **1998**, *258*, 1–14. [CrossRef]
- Stoloff, N.S.; Liu, C.T.; Deevi, S.C. Emerging applications of intermetallics. *Intermetallics* **2000**, *8*, 1313–1320. [CrossRef]
- Wang, J.; Xing, J.; Qiu, Z.; Zhi, X.; Cao, L. Effect of fabrication methods on microstructure and mechanical properties of Fe₃Al-based alloys. *J. Alloys Compd.* **2009**, *488*, 117–122. [CrossRef]
- Schneider, A.; Falat, L.; Sauthoff, G.; Frommeyer, G. Microstructures and mechanical properties of Fe₃Al-based Fe-Al-C alloys. *Intermetallics* **2005**, *13*, 1322–1331. [CrossRef]
- Abel, A. Ambient and High-Temperature Mechanical Properties of Intermetallic Fe₃Al Alloys with Complex Borides. 2022. Available online: <https://opus4.kobv.de/opus4-bam/frontdoor/index/index/docId/55993> (accessed on 23 February 2024).
- Zhao, J.; Xu, G.; Wang, Z.; Ju, J.; Wang, X.; Chen, M.; Xue, F.; Zhou, J. Effect of weaving on Fe₃Al layers prepared by arc deposition technique. *J. Mater. Eng. Perform.* **2024**, *33*, 706–723. [CrossRef]
- Abel, A.; Rosalie, J.M.; Reinsch, S.; Zapala, P.; Michels, H.; Skrotzki, B. Influence of Mo and B additions in intermetallic near-Fe₃Al alloys on microstructure and mechanical properties. *Intermetallics* **2023**, *163*, 108074. [CrossRef]
- Qian, Z. Preparation and Tribological Properties of Fe₃Al-Al₂O₃ Composite Materials. Master's Thesis, Lanzhou University of Technology, Lanzhou, China, 2013.
- Li, W.; Zhang, Y. Study on the segregation of B at grain boundaries in intermetallic compound Ni₃Al. *Min. Metall. Eng.* **1999**, *19*, 69–70.
- Liu, Y.; Huang, Y.; Gao, T.; Li, C.; Hou, J.; Huang, R. Synergistic effect of Mn and B on the cohesive properties of grain boundaries in Ni₃Al: A first-principles study. *Mater. Today Commun.* **2024**, *38*, 108055. [CrossRef]
- Cao, S.; Liang, J.; Wang, L.; Zhou, J. Effects of NiCr intermediate layer on microstructure and tribological property of laser cladding Cr₃C₂ reinforced Ni60A-Ag composite coating on copper alloy. *Opt. Laser Technol.* **2021**, *142*, 106963. [CrossRef]
- Guo, Z.; Zhang, A.; Han, J.; Meng, J. Microstructure, mechanical and tribological properties of CoCrFeNiMn high entropy alloy matrix composites with addition of Cr₃C₂. *Tribol. Int.* **2020**, *151*, 106436. [CrossRef]
- Su, Z.; Li, J.; Shi, Y.; Ren, S.; Zhang, Z.; Wang, X. Effect of process parameters on microstructure and tribological properties of Ni60A/Cr₃C₂ laser cladding on 60Si2Mn steel. *Surf. Coat. Technol.* **2023**, *473*, 130005. [CrossRef]
- Urtekin, L.; Gunes, D.; Yilan, F.; Çanl, M. The Effect of Layers on the Unidirectional Carbon Fibers of the Reinforced Polyester Resin Matrix Composite Material. *Gazi Univ. J. Sci. Part C Des. Technol.* **2021**, *10*, 495–503. [CrossRef]
- Yuan, Y.; Liu, H.; Huang, Z. Effect of Cr₃C₂ content on the microstructure and mechanical properties of hot-pressed sintering WC-based cemented carbide materials. *Powder Metall. Mater. Sci. Eng.* **2023**, *28*, 55–62.
- Liu, Z.; Yin, F.; Chen, C.; Zhao, L.; Fu, L.; Feng, Y.; Cao, Y.; Peng, Y.; Tian, Z.; Li, C. Microstructure and Wear Resistance of a Cr₇C₃ Reinforced Ni₃Al Composite Coating Prepared by Laser Cladding. *Coatings* **2022**, *12*, 105. [CrossRef]
- Li, M.; Han, B.; Song, L.; He, Q. Enhanced surface layers by laser cladding and ion sulfurization processing towards improved wear-resistance and self-lubrication performances. *Appl. Surf. Sci.* **2020**, *503*, 144226. [CrossRef]
- Zhu, L.; Xue, P.; Lan, Q.; Meng, G.; Ren, Y.; Yang, Z.; Xu, P.; Liu, Z. Recent research and development status of laser cladding: A review. *Opt. Laser Technol.* **2021**, *138*, 106915. [CrossRef]
- Tamanna, N.; Crouch, R.; Naher, S. Progress in numerical simulation of the laser cladding process. *Opt. Lasers Eng.* **2019**, *122*, 151–163. [CrossRef]
- Feng, Y.; Shan, J.; Zhao, L.; Liu, Z.; Gong, K.; Li, C. Effect of Cr₃C₂ Content on the Microstructure and Wear Resistance of Fe₃Al/Cr₃C₂ Composites. *Coating* **2022**, *12*, 1980. [CrossRef]
- Zhao, G.; Zhang, J.; Song, Y.; Li, J.; Li, H.; Shuai, M. Research on the friction and wear properties of the wear-resistant layer of NM500/Q345 composite plates under different quenching temperatures. *Precis. Form. Eng.* **2021**, *13*, 35–41.
- Gao, C. The Relationship between Hardness and Wear Resistance of Metals. *Mech. Eng.* **1981**, *4*, 6–8.

25. Hu, Y.; Watson, M.; Maiorino, M.; Zhou, L.; Wang, W.; Ding, H.; Lewis, R.; Meli, E.; Rindi, A.; Liu, Q.; et al. Experimental study on wear properties of wheel and rail materials with different hardness values. *Wear* **2021**, *477*, 203831. [[CrossRef](#)]
26. Yuan, Y.; Li, Z. Effects of rod carbide size, content, loading and sliding distance on the friction and wear behaviors of $(\text{Cr, Fe})_7\text{C}_3$ reinforced α -Fe based composite coating produced via PTA welding process. *Surf. Coat. Technol.* **2014**, *248*, 9–22. [[CrossRef](#)]
27. Hu, J.; Li, D.; Llewellyn, R. Computational investigation of microstructural effects on abrasive wear of composite materials. *Wear* **2005**, *259*, 6–17. [[CrossRef](#)]

Disclaimer/Publisher’s Note: The statements, opinions and data contained in all publications are solely those of the individual author(s) and contributor(s) and not of MDPI and/or the editor(s). MDPI and/or the editor(s) disclaim responsibility for any injury to people or property resulting from any ideas, methods, instructions or products referred to in the content.